An Assessment of Additively Manufactured Bonded Permanent Magnets for a Distributed Wind Generator

Preprint

C. J. J. Labuschagne,[1] L. Sethuraman,[1] T. Hanley,[2] M. P. Paranthaman,[3] and L. J. Fingersh[1]

1 National Renewable Energy Laboratory
2 Bergey Windpower Co.
3 Oak Ridge National Laboratory

Presented at International Electric Machines and Drives Conference (IEMDC)
San Francisco, California
May 15–18, 2023

NREL is a national laboratory of the U.S. Department of Energy
Office of Energy Efficiency & Renewable Energy
Operated by the Alliance for Sustainable Energy, LLC

This report is available at no cost from the National Renewable Energy Laboratory (NREL) at www.nrel.gov/publications.

Contract No. DE-AC36-08GO28308

Conference Paper
NREL/CP-5000-85626
September 2023

An Assessment of Additively Manufactured Bonded Permanent Magnets for a Distributed Wind Generator

Preprint

C. J. J. Labuschagne,[1] L. Sethuraman,[1] T. Hanley,[2] M. P. Paranthaman,[3] and L. J. Fingersh[1]

1 National Renewable Energy Laboratory
2 Bergey Windpower Co.
3 Oak Ridge National Laboratory

Suggested Citation
Labuschagne, C. J. J., L. Sethuraman, T. Hanley, M. P. Paranthaman, and L. J. Fingersh. 2023. *An Assessment of Additively Manufactured Bonded Permanent Magnets for a Distributed Wind Generator: Preprint*. Golden, CO: National Renewable Energy Laboratory. NREL/CP-5000-85626. https://www.nrel.gov/docs/fy23osti/85626.pdf.

NREL is a national laboratory of the U.S. Department of Energy
Office of Energy Efficiency & Renewable Energy
Operated by the Alliance for Sustainable Energy, LLC

This report is available at no cost from the National Renewable Energy Laboratory (NREL) at www.nrel.gov/publications.

Contract No. DE-AC36-08GO28308

Conference Paper
NREL/CP-5000-85626
September 2023

National Renewable Energy Laboratory
15013 Denver West Parkway
Golden, CO 80401
303-275-3000 • www.nrel.gov

NOTICE

This work was authored in part by the National Renewable Energy Laboratory, operated by Alliance for Sustainable Energy, LLC, for the U.S. Department of Energy (DOE) under Contract No. DE-AC36-08GO28308. Funding provided by U.S. Department of Energy Office of Energy Efficiency and Renewable Energy Wind Energy Technologies Office. The views expressed herein do not necessarily represent the views of the DOE or the U.S. Government. The U.S. Government retains and the publisher, by accepting the article for publication, acknowledges that the U.S. Government retains a nonexclusive, paid-up, irrevocable, worldwide license to publish or reproduce the published form of this work, or allow others to do so, for U.S. Government purposes.

Cover Photos by Dennis Schroeder: (clockwise, left to right) NREL 51934, NREL 45897, NREL 42160, NREL 45891, NREL 48097, NREL 46526.

An Assessment of Additively Manufactured Bonded Permanent Magnets for a Distributed Wind Generator

C. J. J. Labuschagne
National Renewable Energy Laboratory
National Wind Technology Center
Golden, Colorado
hannes.labuschagne@nrel.gov

L. Sethuraman
National Renewable Energy Laboratory
National Wind Technology Center
Golden, Colorado
latha.sethuraman@nrel.gov

T. Hanley
Bergey Windpower Co.
Norman, Oklahoma
thanley@bergey.com

M. P. Paranthaman
Oak Ridge National Laboratory
Oak Ridge, Tennessee
paranthamanm@ornl.gov

L. J. Fingersh
National Renewable Energy Laboratory
National Wind Technology Center
Golden, Colorado
lee.fingersh@nrel.gov

***Abstract*—In this paper, we examine and compare the performance of a generator design optimized using additively manufactured NdFeB–SmFeN in nylon-polymer-bonded permanent magnets (PMs) against a generator design with conventional NdFeB sintered PMs. To realize this, a commercially available 15-kW wind generator's rotor is re-optimized using both additively manufactured and sintered NdFeB magnets using simple geometric parameterization that allowed for two specific magnet shapes, namely, arc-shaped and crown-shaped designs. Results showed that for a similar generator performance, the designs with additively manufactured bonded PMs are more cost-competitive in terms of the estimated PM material cost and also have negligible eddy current magnet losses.**

***Index Terms*—additive manufacturing, permanent magnet, wind energy, wind generator.**

I. INTRODUCTION

Direct-drive permanent magnet synchronous generators (PMSGs) account for a significant share of small and distributed wind turbines that are installed for off-grid systems and certain specialized applications in the United States. As new installations for small wind turbines are growing to be more expensive per kilowatt installed [1], the price volatility of raw materials and rare earth permanent magnet (PM) materials (e.g., NdFeB) that are needed to enable these systems is challenging their commercial attractiveness. A key interest for small-wind-turbine manufacturers has been producing low-cost, efficient, and reliable generator technologies by using design optimization methods to minimize PM mass [2] and to enable those designs by means of cost-competitive manufacturing [3]. This includes the use of rare-earth-free magnets (e.g, ferrites) or reduced rare earth M-, H- or SH-grade magnets that provide the designs with a cost advantage through reduced dysprosium content.

As yet, most wind generator designs are radial flux topology generators that use conventional arc-shaped magnets, which could limit the opportunities for material savings. At the same time, new manufacturing methods such as additive manufacturing (AM) [4], and new design techniques [5] are emerging for electric machines. For instance, magnet shaping has been shown to improve torque quality and affect the average torque in some cases [6] [7], and with the design freedom that the AM process allows, it is worth re-exploring the design space. Moreover, as the properties of most AM bonded magnets continue to improve [8], with the most advanced magnets having an energy product of 20 MGOe (MegaGaussOersteds) [9], newer designs enabled by shape freedom of AM can result in an improved performance with weaker materials. AM bonded magnets also offer some potential performance-related advantages when compared to sintered NdFeB: (i) these magnets have a much higher resistivity and therefore tend to result in reduced eddy current magnet losses, and (ii) they can operate at much higher temperatures without partial irreversible demagnetization. Because some of these magnets are also dysprosium-free, this presents an opportunity to reduce material costs by near-net shaping, and the final geometry can be achieved with little to no need for machining.

Inspired by these advantages, as part of the DOE sponsored MADE3D program [10], we investigate the potential for cost savings with AM magnets for a baseline distributed wind turbine generator modeled around Bergey Windpower Co.'s 15-kW turbine system. We explore alternative magnet shapes by parameterizing arc-shaped and crown-shaped magnets using state-of-the-art AM bonded magnets. Owing to the commercial nature of the baseline generator design, certain sensitive information around the design are deemed as proprietary and not disclosed. As part of the design optimization, we investigate two approaches: (i) replacing the NdFeB sintered magnets with AM bonded magnets and (ii) replacing the arc-shaped magnets with crown-shaped magnets. All investigations involved magneto-thermal finite-element evaluations using commercial finite element analysis (FEA) software, Altair FLUX [11].

Funding provided by the U.S. Department of Energy Office of Energy Efficiency and Renewable Energy Wind Energy Technologies Office.

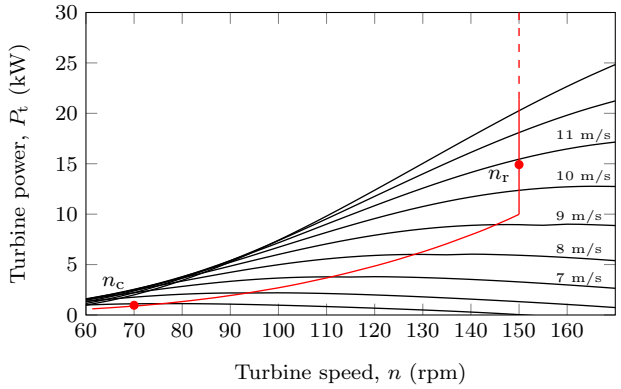

Fig. 1. Turbine power versus speed curves with specified operation.

II. SYSTEM DESCRIPTION AND SPECIFICATIONS

In this section, a brief description of the 15-kW distributed wind energy system and an overview of the specifications are given.

A. Turbine Specifications

The wind turbine power versus speed curves are shown in Fig. 1 along with the generator's power curve for the desired operation. As shown in Fig. 1, the generator cuts in at a turbine speed of $n_c = 70$ rpm and a wind speed of 4 m/s. The rated operating point of 15 kW is at $n_r = 150$ rpm and a wind speed ≈ 11 m/s. The maximum turbine speed is limited to $n = 150$ rpm and the minimum required stalling power from the generator for electromagnetic braking is $P_{stall} = 40$ kW. These specifications are summarized in Table I.

B. Drivetrain Specification

A simplified single-line diagram of the 15-kW drivetrain is shown in Fig. 2. In Fig. 2, the PMSG is connected to the grid via a back-to-back, full-rated frequency converter. (In the system used by Bergey Windpower Co., a three-phase diode bridge rectifier with a grid-tie converter is used; for simplicity in the design and analysis, and because such an implementation did not significantly detract from the main conclusions relating to the research question, we opt for the system as shown in Fig. 2.) In addition, the generator is connected to a dump-load resistor bank via a silicon controlled rectifier (SCR) that forms a part of the electromagnetic braking system. This particular wind turbine has fixed-pitch blades and does not have a furling or yaw control system. Therefore, the system relies on the previously mentioned electromagnetic braking system to reduce the turbine speed. This way, the braking system protects the power electronics from overcurrent damage during operation and stops the turbine from speed-up and runaway (i.e., stalling) during extreme weather conditions.

C. PM Wind Generator

The partial cross section of the baseline wind generator is shown in Fig. 3. The generator is a radial-flux, outer-rotor surface-mounted PMSG and has a fractional-slot concentrated winding with a slot-pole combination of 60-50.

TABLE I
SUMMARY OF SPECIFIED OPERATING POINTS.

	n_c	n_r
Wind speed	4 m/s	11 m/s
Turbine speed	70 rpm	150 rpm
Generated power, P_{rated}	0 kW	15 kW
Stalling power output, P_{stall}	-	$\geq$ 40 kW

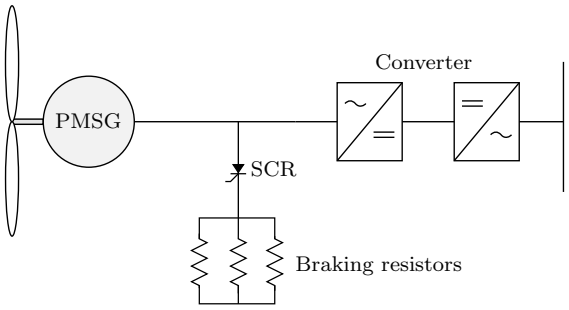

Fig. 2. Single line diagram of the direct-drive PMSG wind energy system with active control and passive electric braking.

III. ADDITIVELY MANUFACTURED PERMANENT MAGNETS

The magnets used in the baseline generator shown in Fig. 3 are standard NdFeB N48H-grade sintered magnets. This magnet grade is very attractive for small-scale distributed wind generators due to its high energy product and relatively low demagnetizing knee point. The maximum operation temperature for N48H-grade magnets is 120 °C. The normal B-H curves for these N48H-grade magnets were obtained from [12] and are also shown in Fig. 4. These N48H-grade sintered magnets form the basis of the comparison against the AM bonded magnets.

A. Additive Manufacturing Method

The AM magnets used in the present study are composite magnets made from 75 vol% Magfine NdFeB–SmFeN in nylon-polymer-bonded magnets that were developed at Oak Ridge National Laboratory. These highly dense and magnetically anisotropic rare-earth-free bonded magnets are fabricated via a batch extrusion process described in [13]. To summarize, either a batch mixer or a high-throughput twin screw extruder are used for melt processing and compounding. The simplified schematic in Fig. 5 that is adapted from [13] shows this initial part of the additive manufacturing

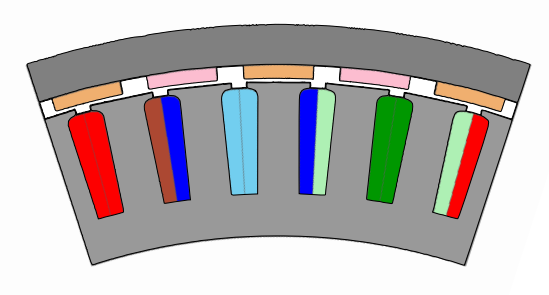

Fig. 3. Partial cross section of the baseline 15-kW Bergey Windpower Co. outer-rotor surface-mounted PM synchronous generator.

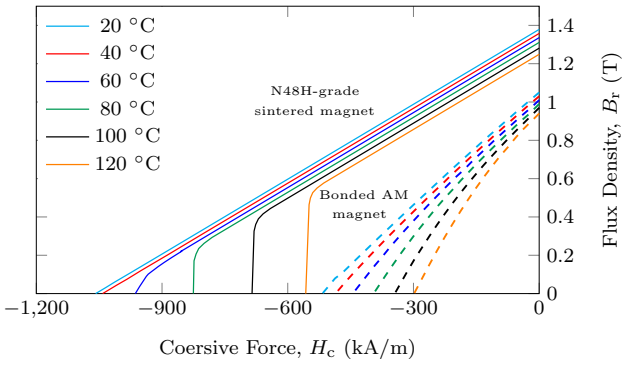

Fig. 4. Demagnetization curves for the N48H-grade NdFeB magnets and 75 vol% NdFeB–SmFeN printed bonded magnets shown as a function of magnet temperature.

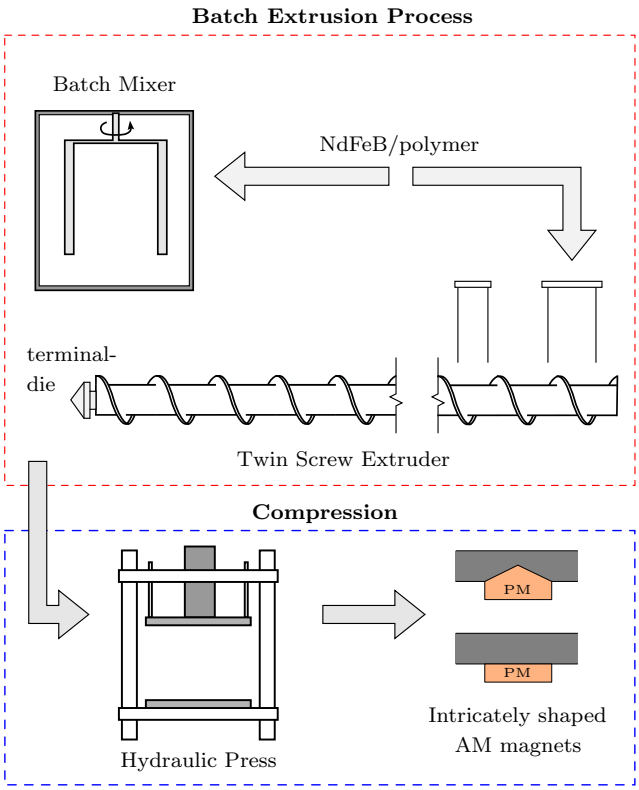

Fig. 5. Simplified schematic of the additive manufacturing process for the 75 vol% NdFeB–SmFeN magnets. (Adapted from [13].)

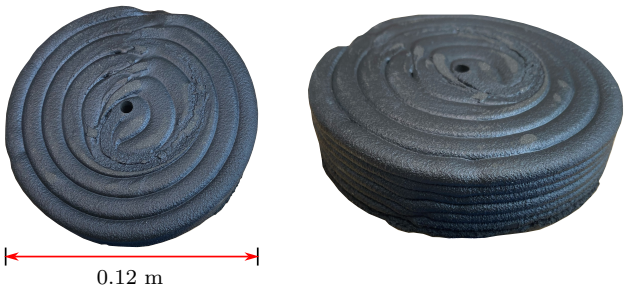

Fig. 6. Raw sample of an AM 75 vol% NdFeB–SmFeN magnet used to measure B-H curves.

TABLE II
SUMMARY OF N48H-GRADE NdFeB SINTERED MAGNET AND 75 VOL% NdFeB–SmFeN AM MAGNET PROPERTIES AT 313.15 K.

	N48H NdFeB	**75 vol% NdFeB-SmFeN**
B_r, (T)	1.36	1.03
H_{ci} (intrinsic), (kA/m)	1,200.0	859.4
H_c (normal), (kA/m)	1,041.7	485.9
BH_{max}, (MGOe)	45	20
Density, (kg/m^3)	7,600	6,150
Resistivity, (Ω·m)	1.5×10^{-6}	0.0258

process. The polymer binder and magnet powder are added to the batch mixer at various stages under optimized conditions. Once a uniform melt is achieved, the mixture is extruded through a die. For the twin screw extruder, the polymer binder and magnet powder are fed into the extruder at various zones under optimized conditions and feeding rates. The compound is also then extruded through a die. The NdFeB/polymer compounds produced by this initial part of the process are then compressed into near-net magnet shapes onto the rotor using 3D-printed mold by indirect additive manufacturing. Alternatively, machining can be incorporated into the postprocessing stage to achieve the desired magnet shape. Thereafter, the magnetic alignment of the near-net-shape magnets is achieved through a post magnetic annealing process, where an external magnetic field of 1.5 T is applied at a temperature of 590 K.

B. Material Properties

The feedstock in Fig. 5 consisted of 96 wt.% anisotropic Magfine NdFeB and SmFeN magnet powders, blended with 4 wt.% nylon polymer binder. The hybrid bonded magnet with 75 vol% magnet loading yielded a bulk density of 6,150 kg/m^3 and shows excellent measured magnetic properties, with a B_r of 1.04 T, an intrinsic coercivity H_{ci} of 859.4 kA/m, and a BH_{max} of 20 MGOe at 300 K. The normal B-H curves for these magnets at different magnet temperatures were obtained by curve-fitting and interpolation of data from raw measurements and are shown in Fig. 4 (dashed lines). For these measurements, coupon-sized magnets measuring $152.4 \times 152.4 \times 8$ mm^3 were used; a raw sample of an AM magnet is shown in Fig. 6.

The main properties of the N48H-grade NdFeB and the AM magnet are summarized in Table II. Note that the printed PMs have a resistivity of $\rho = 0.0258$ Ω·m and the N48H-grade PMs have a resistivity of $\rho = 1.5 \times 10^{-6}$ Ω·m, which indicates that magnet eddy current losses in the AM magnets will be significantly reduced. Another advantage of these 75 vol% Magfine NdFeB–SmFeN bonded magnets is that the magnetic properties are superior to any commercially available bonded NdFeB magnets that are obtained by injection molding [13]. The tensile strength properties of the AM magnets were measured in [13] and are in the range of 32–52 MPa. Moreover, in the cases where the AM magnets are either directly compressed onto the outer rotor can or where an adhesive is used to apply the magnets, this mechanical strength will be adequate to withstand any centrifugal forces experienced during operation.

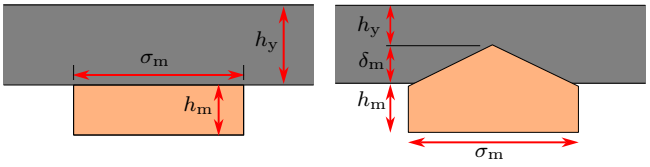

(a) (b)

Fig. 7. Partial rotor cross-sectional sketches illustrating the relevant dimensions for the design optimization: (a) arc-shaped magnet; (b) crown-shaped magnet.

C. Demagnetization Threshold for AM Magnets

The demagnetization threshold for magnets can typically be determined from the normal B-H curves as shown in Fig. 4. However, the B-H curves for the AM magnets are near linear, and there is no clear knee point for any of the temperatures at which the respective B-H curves were measured. It is also assumed that the steady-state operating temperature of the magnets will not exceed $T_{\text{PM}} = 60$ °C. We made an assumption that at lower temperatures, i.e., $T_{\text{PM}} \leq 60$ °C, the knee point for AM magnets is between $B_{\text{r}} = 0.2$ T and 0.4 T. It is anticipated that in this zone, the magnet can reasonably retract the hysteresis path. In this investigation, the minimum allowable remnant flux density in the AM magnets during any operation is taken as $B_{\text{r-min}} = 0.3$ T.

IV. Design Optimization

In this section, an overview of the design and optimization approach for the 15-kW PMSG using the different magnet types is given.

We chose to retain the stator design of the baseline generator and only alter the rotor yoke and PM dimensions for the optimization. For the magnets, we chose to parameterize a simple arc-shaped magnet using its height and pole pitch. As a second option, we chose to add an additional design freedom that allowed the magnet to grow in height in the center assuming the shape of a crown. Fig. 7(a) and (b) show the partial cross sections of the rotor with a conventional arc-shaped magnet and a crown-shaped magnet. The geometric variables for the optimization are also defined in Fig. 7. Altogether then, four magnet material–magnet designs are optimized in this paper. They are (i),(ii) the conventional arc-shaped magnet and crown-shaped magnet with the N48H-grade NdFeB magnet material, and (iii),(iv) the conventional arc-shaped magnet and crown-shaped magnet with the 75 vol% NdFeB–SmFeN AM bonded magnet material. For the cases where the AM magnets are used, the magnets are compressed to the printed rotor can. The printed rotor can's material properties are comparable to 1020 steel.

In modeling the generator, we chose to model only a partial section of the machine with an odd periodicity boundary condition (5 poles and 6 slots). Considering the multiphysics problem, this greatly simplified the analyses and was sufficient to capture the performance sensitivities at a reasonable level of fidelity and accuracy. The machine was assumed to be cooled by natural air convection so that the maximum winding current density was limited to 6 A/mm^2. A key goal of the design optimization was to vary the dimensions of the magnets that minimized the PMSG's

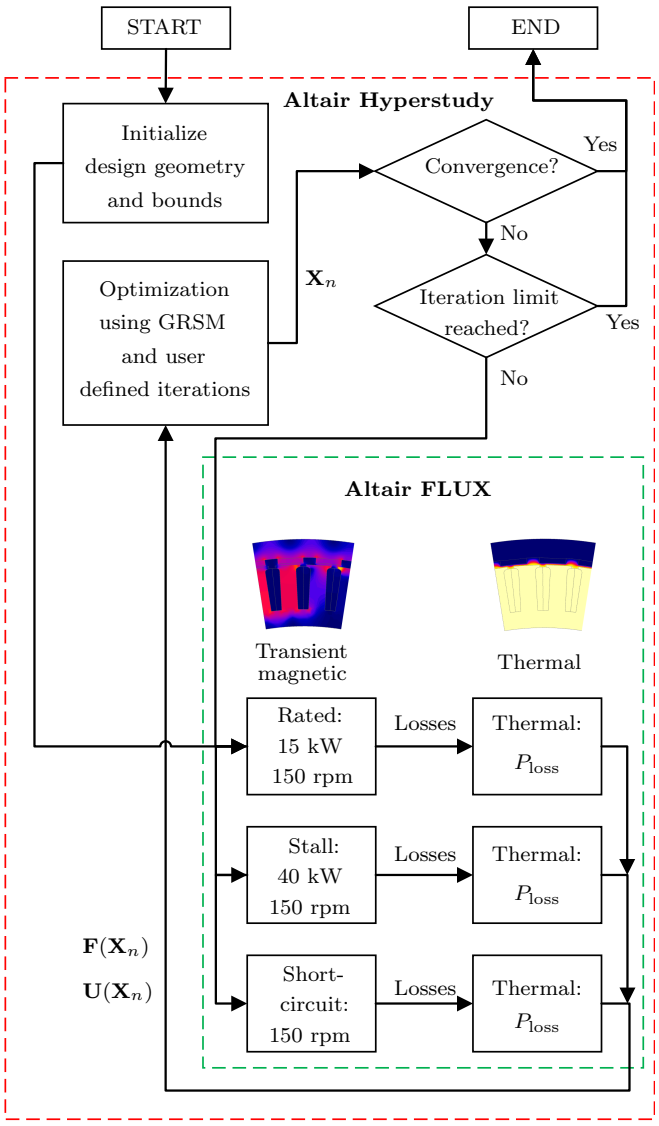

Fig. 8. Simulation and optimization workflow as carried out using Altair Hyperstudy and FLUX.

magnet mass and/or costs, M_{PM}, while still adhering to some performance constraints and the system's specifications that were outlined in Section II. For the design optimization, the Global Response Surface Method (GRSM) from [14] is used, where multiple iterations of design of experiments are performed using different magnet dimensions. For each design the performance was evaluated by transient magnetic FEA followed by a steady-state thermal analysis, and the best design from each iteration guided the search toward the most optimal design. The design constraints are given by

$$\begin{aligned} &\min \{\mathbf{F}(\mathbf{X}_n) = M_{\text{PM}}(\mathbf{X}_n)\}, \\ &\text{s.t. } \{\mathbf{U}(\mathbf{X}_n)\ [P_{\text{rated}} = 15 \text{ kW},\ \eta \geq 96\ \%, P_{\text{stall}} \geq 40 \text{ kW}, \\ &B_{\text{r-min}} \geq 0.45 \text{ T or } 0.3 \text{ T}, T_{\text{Cu}} \leq 180°\text{C},\ \tau_{\text{cog}} \leq 25 \text{ Nm}\ ]\}, \end{aligned} \tag{1}$$

where $\mathbf{X}_n$ is the input vector with the respective rotor's dimensions as defined in Fig. 7(a) or (b). The lower and upper bounds of the dimensions are given in Table III.

In equation (1), P_{rated} is the generator's output power at the rated operating point and η is the generator's efficiency

TABLE III
LOWER AND UPPER BOUNDS FOR THE RESPECTIVE ROTOR'S DIMENSIONS.

	Unit	Lower	Upper
Conventional magnet:			
h_{m} - magnet height	mm	3.0	7.0
σ_{m} - magnet pitch-to-pole pitch ratio	p.u.	0.65	0.85
h_{y} - rotor yoke height	mm	8.0	18.0
Crown-shaped magnet:			
h_{m} - magnet height	mm	3.0	7.0
σ_{m} - magnet pitch to pole pitch ratio	p.u.	0.65	0.85
h_{y} - rotor yoke height	mm	5.0	18.0
δ_{m} - magnet crown height	mm	-4.0	5.0

at the rated operating point given by

$$\eta = \frac{P_{\text{out}}}{P_{\text{out}} + P_{\text{loss}}} \times 100 = \frac{P_{\text{out}}}{P_{\text{out}} + P_{\text{Cu}} + P_{\text{Stator}} + P_{\text{Rotor}} + P_{\text{PM}}} \times 100. \quad (2)$$

In equation (2), the generator efficiency is calculated by taking into account the winding's copper losses, P_{Cu}, the stator iron losses, P_{Stator}, the joule losses in the solid rotor can, P_{Rotor}, and the eddy current losses in the PMs, P_{PM}. The other constraints in equation (1) are the generator's maximum output power during stalling, P_{stall}; the minimum remnant flux density in the PMs during any operation, $B_{\text{r-min}}$, to account for permanent PM demagnetization (in equation (1), $B_{\text{r-min}} \geq 0.3$ T for AM PMs); the maximum winding temperature during rated operation, T_{Cu}, as a thermal constraint; and the generator's cogging torque, τ_{cog}.

From the above design objectives and constraints, the generator solution in the optimization is solved for rated operation, during stalling and also during a three-phase symmetric short-circuit fault condition. A thermal analysis is also done for each of these conditions for each solution. The optimization workflow is shown in Fig. 8. For the steady-state thermal analysis, the losses calculated in the electromagnetic analysis P_{Cu}, P_{Stator}, P_{Rotor}, and P_{PM} are assigned to the respective component regions and are assumed to be equally distributed. The thermal convection coefficient applied to the inner boundary of the stator is that of static air h = 2.5 W/m^2·K. At the outer boundary of the rotor and the air gap, a thermal convection coefficient of h = 33.19 W/m^2·K is applied. This corresponded to the heat transfer coefficient of air flowing at a velocity of approximately 11 m/s at rated turbine speed of 150 rpm [15]. For all of the designs in the optimization, the ambient temperature is taken as 40 °C. The stator windings have an H-grade insulation, so the maximum temperature rise was limited to 180 °C.

V. OPTIMIZATION RESULTS

The results from the optimization and the performance parameters of the baseline generator are summarized in Table IV. Also given in Table IV are the estimated PM material costs for each rotor design, C_{PM}. Considering the uncertainty in magnet material prices, we estimate the material costs C_{PM} with a per-unit value. The material costs for the 75 vol% AM PMs are 0.55 pu compared to 1.0 pu for the N48H NdFeB PMs. (Manufacturing and labor costs are difficult to estimate at this time and are not included.)

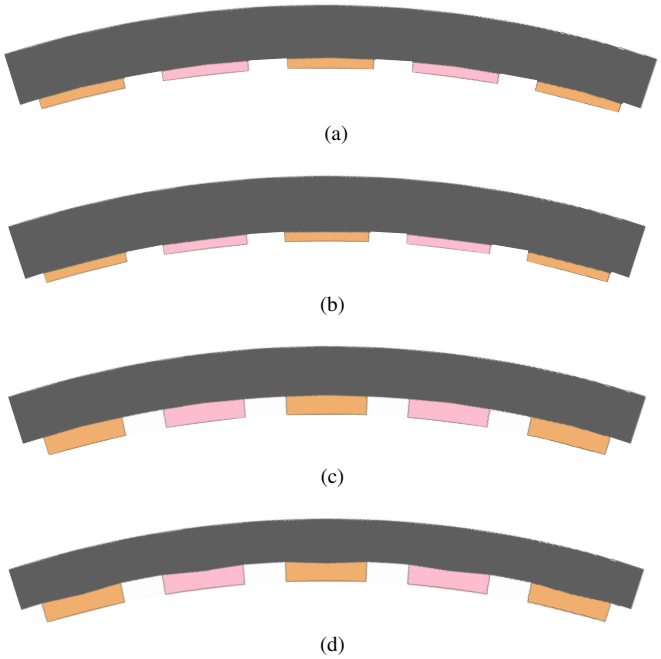

Fig. 9. Rotor cross sections of the optimized machines for (a) the N48H NdFeB conventional arc-shaped magnet, (b) the N48H NdFeB crown-shaped PM, (c) the 75 vol% NdFeB–SmFeN arc-shaped PM (d) the 75 vol% NdFeB–SmFeN crown-shaped PM.

In terms of the design objective, it is shown in Table IV that the optimized designs with the N48H-grade magnets use between 24% and 30% less PM material than the optimized designs with the AM magnet material. This is an expected result, and it is shown in Fig. 10 with the air-gap flux density plots obtained from the FEA solutions that a higher air-gap flux density is achieved for the designs using the stronger N48H sintered magnets. Despite the weaker magnet properties of the AM magnets, the torque insufficiency is compensated for by marginally drawing more currents in the windings using a full-rated power converter. The resulting designs are heavier than the designs with N48H-grade magnets. The maximum no-load air-gap flux density values, B_{g}, and the per unit stator current values, I_{peak}, are given in Table IV. In terms of magnet shaping, an interesting result is that the crown-shaped designs resulted in a negative crown height on the rear side for both sintered and AM magnets. A slight mass reduction is found to be possible with the crown-shaped design. This can be attributed to the design freedom allowed by AM through magnet shaping. In this case, the negative crown height resulted in a reduced magnet material mass without compromising the performance of the generator. This is shown with the partial rotor sketches in Fig. 9. Lastly, up to 13% reduction of PM material costs also appears to be possible when using AM magnets.

Despite the relative mass increase with AM magnets, based on the generator performance at rated conditions and the estimated PM material cost, it is shown in Table IV that the designs using the 75 vol% NdFeB–SmFeN AM bonded magnet material are competitive with the designs that use the N48H-grade NdFeB sintered magnet material: the efficiencies for all of the designs are greater than 96% with

TABLE IV
DESIGN OPTIMIZATION RESULTS FROM GRSM

Material		**N48H NdFeB**		**75 vol% NdFeB–SmFeN**	
Magnet shape	Baseline	Conv.	Crown	Conv.	Crown
h_{m} (mm)		3.0	3.0	5.62	5.89
σ_{m} (p.u.)		0.69	0.689	0.658	0.658
h_{y} (mm)		15.09	16.48	14.4	10.8
δ_{m} (mm)		-	-0.21	-	-0.626
M_{PM} (p.u.)	1.0	0.59	0.56	0.85	0.84
C_{PM} (p.u.)	1.0	0.59	0.56	0.47	0.46
P_{rated} (kW)		15.0	15.0	15.0	15.0
η (%)		96.9	96.1	97.1	97.1
P_{stall} (kW)		40.0	40.0	40.0	40.0
$B_{\mathrm{r\text{-}min}}$ (T)		0.456	0.453	0.302	0.304
T_{Cu} (°C)		73.6	73.4	74.2	74.5
τ_{cog} (Nm)		24.8	24.7	24.1	24.0
Loss breakdown:					
- P_{PM} (W)		54.5	55.4	0.005	0.005
- P_{Stator} (W)		249.2	239.1	168.2	165.7
- P_{Rotor} (W)		110.2	122.4	110.6	115.3
- P_{Cu} (W)		171.0	180.1	265.5	271.1
B_{g} (T)		1.02	1.11	0.87	0.85
I_{peak} (p.u.)	1.0	1.17	1.20	1.46	1.47
T_{PM} (°C)		54.5	55.4	48.5	48.8
$T_{\mathrm{Cu\text{-}SC}}$ (°C)		208.0	196.9	156.5	155.2

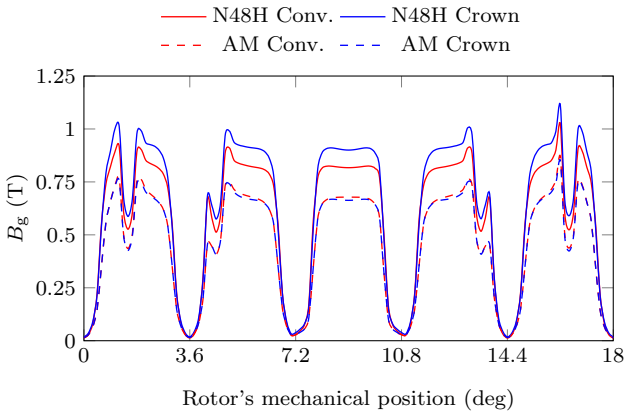

Fig. 10. FEA-predicted air-gap flux density for the optimized designs.

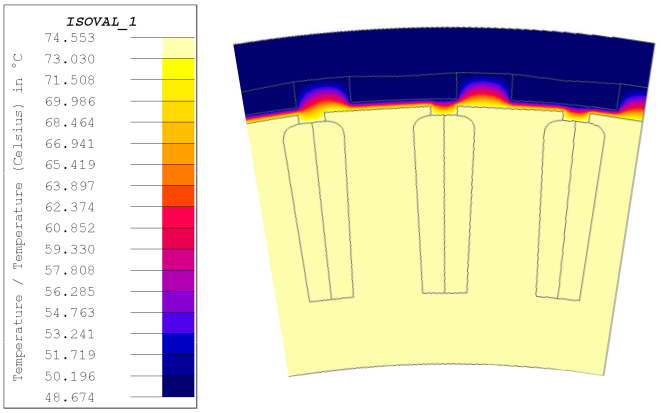

(a)

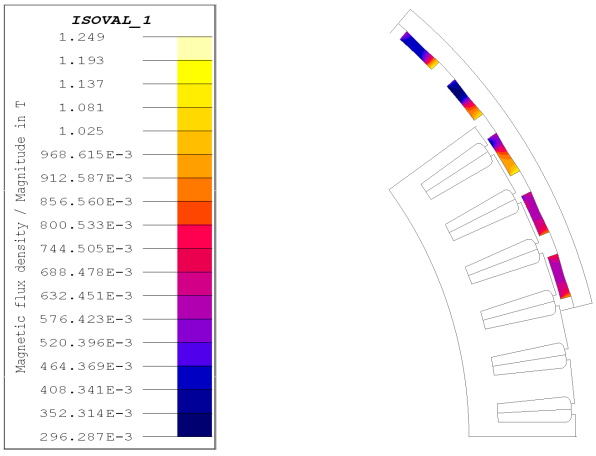

(b)

Fig. 11. (a) Thermal analysis result of the optimized crown-shaped 75 vol% NdFeB–SmFeN AM magnet rotor at rated power. (b) Minimum remnant flux density contour plot of the optimized crown-shaped 75 vol% NdFeB–SmFeN AM magnet rotor during stalling.

little variation; the generator cogging torque is lower than that of the specified maximum; all of the optimized magnet designs are at low risk of partial irreversible demagnetization, even during a short-circuit fault; and all of the designs meet the generator stalling output power requirement for P_{stall}.

Another noteworthy result given in Table IV is the magnet losses, P_{PM}, and it is shown that for the AM magnets $P_{\mathrm{PM}} \approx 0$ W. This is due to the much greater resistivity of the AM magnets when compared to that of the N48H-grade sintered magnets, as discussed in Section III. As a result, when using AM magnets these negligible magnet losses help compensate for the higher copper losses in the windings.

Also given in Table IV are the steady-state temperatures of the magnets, T_{PM}, at rated power. It is thus shown for both magnet types that the difference in steady-state temperature at rated power and the assumed ambient temperature, $\Delta T = T_{\mathrm{PM}} - T_{\mathrm{amb}}$, is less than $\Delta T = 20$ °C. To better illustrate

these results, the temperature plot of the optimized crown-shaped 75 vol% NdFeB–SmFeN AM magnet rotor from the thermal analysis at rated power is shown in Fig. 11(a). In addition, the FEA magnetic flux density contour plot showing the minimum remnant flux density in the magnets ($B_{\text{r-min}}$) during stalling is given in Fig. 11(b). This confirms that the $B_{\text{r-min}}$ constraints in Table IV are met. Finally, the steady-state temperatures of the windings during a short-circuit fault, $T_{\text{Cu-SC}}$, are also given in Table IV (note that this condition would only occur during an uncleared fault). In this case, for the designs using the AM magnets, $T_{\text{Cu-SC}}$ is still below the maximum temperature for the winding's H-grade insulation class. For the designs using the N48H-grade magnets, $T_{\text{Cu-SC}}$ is near 200 °C, which is still acceptable.

The results show that the optimized designs with crown-shaped magnets offer some mass and cost reduction advantages (both using NdFeB and AM magnets). AM can be used for both the magnets and the rotor can. For the AM bonded magnets, intricately shaped molds can be fabricated using AM, as described in Section III. For the much larger rotor can, AM can also be used in the fabrication process. The shaped rotor with extruding crowns as in Fig. 9(b) and (d) can be realized using binder jetting to fabricate a shaped sand mold for casting. Ultimately, these methods will result in less material wastage and might offer further cost reduction advantages.

VI. Conclusions

The results from the investigation indicate that despite the weaker magnetic properties of AM magnets, by exploring the design freedom and appropriate shaping, it is possible to minimize any additional mass penalties and save costs, which makes them suitable for practical application for a 15-kW wind generator employing a full rated converter in the system. The following observations were made:

- It is shown that the crown-shaped magnets resulted in a marginal magnet mass-reduction advantage. This was possible due to the design freedom that allowed the negative crown height in the magnet designs. However, further investigation with intricately parameterized AM magnet shapes could better exploit the design freedom allowed by AM and provide more insights.
- It is found that the optimized designs using the N48H-grade NdFeB magnets use less magnet material mass than the optimized designs using the AM magnets, which is an expected result. However, with the estimated magnet material cost it is shown that the optimized designs using AM magnets are more cost-competitive while still achieving a similar performance at the specified operating points of the wind energy system, which is compelling for generator manufacturers.
- It is also shown that a key performance advantage of using these AM magnets is that they have negligible eddy current losses.

Acknowledgments

The authors gratefully acknowledge support from Brian Post of Oak Ridge National Laboratory for BAAM printing of magnets and Xubo Liu of Ames Laboratory for magnetic property measurements. Thanks are also due to Lavanya Vadamodalla from Altair for software technical support and troubleshooting. This work was authored in part by the National Renewable Energy Laboratory, operated by Alliance for Sustainable Energy, LLC, for the U.S. Department of Energy (DOE) under Contract No. DE-AC36-08GO28308 and Oak Ridge National Laboratory. Funding provided by the U.S. Department of Energy Office of Energy Efficiency and Renewable Energy Wind Energy Technologies Office. The views expressed in the article do not necessarily represent the views of the DOE or the U.S. Government. The U.S. Government retains and the publisher, by accepting the article for publication, acknowledges that the U.S. Government retains a nonexclusive, paid-up, irrevocable, worldwide license to publish or reproduce the published form of this work, or allow others to do so, for U.S. Government purposes.

References

[1] A. Bianchini, B.-G. I. Galih, Bangga, I.-J. Croce, Alessandro, R. Damiani *et al.*, "Current status and grand challenges for small wind turbine technology," *Wind Energ. Sci.*,, p. 2003–2037, 2022.

[2] G. Bramerdorfer, J. A. Tapia, J. J. Pyrhönen, and A. Cavagnino, "Modern electrical machine design optimization: Techniques, trends, and best practices," *IEEE Transactions on Industrial Electronics*, vol. 65, no. 10, pp. 7672–7684, 2018.

[3] Distributed wind competitiveness improvement project helps manufacturers develop, certify next-gen technologies. Accessed: 2022-12-14. [Online]. Available: https://www.energy.gov/eere/articles/distributed-wind-competitiveness-improvement-project-helps-manufacturers-develop

[4] J. Cui, J. Ormerod, D. Parker, R. Ott, A. Palasyuk, S. Mccall, M. P. Paranthaman, M. S. Kesler, M. A. McGuire, I. C. Nlebedim *et al.*, "Manufacturing processes for permanent magnets: Part I—sintering and casting," *The Journal of The Minerals, Metals Materials Society (TMS)*, pp. 1–17, 2022.

[5] L. Sethuraman, G. Vijayakumar, S. Ananthan, P. Paranthaman, J. Keller, and R. King, "MADE3D: Enabling the next-generation high-torque- density wind generators by additive design and 3D printing," *Forsch Ingenieurwes*, vol. 85, p. 287–311, 2021. [Online]. Available: https://www.osti.gov/biblio/1774852

[6] Z. Chen, C. Xia, Q. Geng, and Y. Yan, "Modeling and analyzing of surface-mounted permanent-magnet synchronous machines with optimized magnetic pole shape," *IEEE Transactions on Magnetics*, vol. 50, no. 11, pp. 1–4, 2014.

[7] G. Devito, S. Nuzzo, D. Barater, M. Soltani, and G. Franceschini, "Combined magnet shaping and asymmetries in surface-mounted permanent magnet machines for improved torque performance," in *2022 International Conference on Electrical Machines (ICEM)*, 2022, pp. 855–861.

[8] H. Tiismus, A. Kallaste, T. Vaimann, and A. Rassõlkin, "State of the art of additively manufactured electromagnetic materials for topology optimized electrical machines," *Additive Manufacturing*, p. 102778, 2022.

[9] H. Wang, T. Lamichhane, and M. Paranthaman, "Review of additive manufacturing of permanent magnets for electrical machines: A prospective on wind turbine," *Materials Today Physics*, p. 100675, 2022.

[10] L. Sethuraman, "T08 – manufacturing and additive design of electric machines enabled by three-dimensional printing (MADE3D)," Tech. Rep., 2021. [Online]. Available: https://www.energy.gov/sites/default/files/2021-10/fy21peerreview-materialsandmanufacturing-nrel-sethuraman.pdf

[11] Altair® flux® applications. Accessed: 2022-12-14. [Online]. Available: https://www.altair.com/flux-applications/

[12] Demagnetization (BH) curves for neodymium magnets. Accessed: 2022-11-04. [Online]. Available: https://www.kjmagnetics.com/bhcurves.asp

[13] K. Mungale, T. N. Lamichhane, H. Wang, B. C. Sales, M. P. Paranthaman, and U. K. Vaidya, "Compression molding of anisotropic ndfeb bonded magnets in a polycarbonate matrix," *Materialia*, vol. 19, p. 101167, 2021.

[14] Altair Hyperstudy Applicaions. Accessed: 2022-12-14. [Online]. Available: https://www.altair.com/hyperstudy-applications

[15] Convective heat transfer. Accessed: 2023-03-10. [Online]. Available: https://www.engineeringtoolbox.com/convective-heat-transfer-d$_4$30.$html$